

OVERVOLTAGE PROTECTION FOR HIGH FREQUENCY HIGH VOLTAGE POWER TRANSFORMERS

Diego Teruo Mendes de Souza¹, Bruno Valverde¹, José Antenor Pomilio²

¹Zasso Brazil, Indaiatuba – SP, Brazil

²University of Campinas, Campinas – SP, Brazil

e-mail: diegoteruomendes@gmail.com, brnovalverde@gmail.com, antenor@fee.unicamp.br

Abstract – Transformers with high-voltage operation may have undesired behavior due to the effects of their parasitic elements. In power electronics applications, if the primary voltage has harmonics, transformer resonances may be excited, causing high primary currents and secondary voltage stress, compromising the device isolation. This behavior is quite dangerous if the transformer operates without load, what means, without damping, because in this situation, the secondary voltage peak can reach more than two times the expected (rated) value. To protect the high frequency high voltage transformer against this dangerous operation, the overvoltage problem in open load condition is carefully explored and explained in this paper, with the proposition of different protection strategies to mitigate its effect, depending on the transformer parasitic elements values. The different strategies are analytically explained and validated by experimental results, showing their criteria design and effectiveness for the protection of high frequency high voltage transformers through the analysis of a 1 kVA, 311V, 20 kHz, 42/512 ferrite core transformer, showing its dynamics working alone and with each protection strategy.

Keywords – High Frequency High Voltage Transformer, Overvoltage Protection, Parasitic Elements, Power Electronics, Resonance Excitation.

I. INTRODUCTION

Transformers are electrical devices of great importance in Electrical Engineering, with typical applications as measurement instruments, electrical insulation, and power transmission [1] [2]. Many aspects are considered for the correct transformer's operation, as its thermal behavior, magnetic coupling, parasitic elements, depending on the application and power transfer. Thus, for the correct design, several models and simulations are adopted [2].

Transformers used in transmission lines operate at 50 or 60 Hz with high voltage ratio, being heavy and bulky. The frequency increase to kHz or MHz reduces considerably the transformer weight and volume, as in high-frequency devices in switched-mode power supplies [3], used with electronic converters that produce waveforms at high frequencies [4].

There are several challenges in high frequency (HF)

transformers design, especially in high voltage (HV) operation because, in this case, it's usual the strong manifestation of parasitics [5] [6] [7] [8] [9]. It's quite difficult getting a general procedure to design these transformers, although specific procedures have been adopted in resonant converters [11] [12] [13] [14] [15] and weed control [16], and different topologies have been explored, as star-core [12] and planar transformers [17] [18].

In some applications the load varies from short-circuit to open-load, unpredictably [16] [19] [20]. When the variation is slow, control strategies can compensate the perturbations [9] [10] [12]. However, if the variation is too fast, the protection must be guaranteed by the transformer itself, avoiding dangerous situations like overcurrents and overvoltages [21].

In [22] the overvoltage problem in the open load condition of HF HV transformers was investigated and some approaches to avoid this effect were considered. Simulations showed the effectiveness of each procedure and they were experimentally validated only in low voltage, low power tests.

A deeper understanding of the strategies is presented in this paper, showing their effectiveness through experimental measurements in high voltage high power applications. Their working and design procedure are showed through analytical approach and waveform analyses. The strategies were developed for a situation in which the load presents a really fast variation, and so the system must react instantaneously to disturbances. Their working principle is showed in a comparative way, highlighting and relating the effectiveness with transformer parameters.

Section I gives a brief introduction, contextualizing and defining the problem; Section II describes the methodology to obtain the transformer parameters; Section III defines and simulates the protection strategies; Section IV derives analytical expressions and shows waveforms that highlight the strategies and the project criteria; Section V shows the experimental results and Section VI concludes the paper.

II. HF HV TRANSFORMER MODEL

Different high frequency models can illustrate the transformer operation. When the interest is the transient behavior and the propagation time is relevant, distributed parameters models can be used [23] [24], otherwise, lumped models are available [25] [26] [27].

A lumped model is showed in Figure 1. The parameters are reflected to the primary side. The windings capacitance

Manuscript received 19/06/2019; first revision 01/08/2019; accepted for publication 25/12/2019, by recommendation of Editor Marcello Mezaroba. <http://dx.doi.org/10.18618/REP.2020.1.0045>

C_p represents the effect of the intrinsic capacitances among the adjacent winding turns and is mainly due to the high number of secondary turns. Other lumped models use additional capacitances and inductances [25] [26] [27]. Besides its simplicity, the lumped model in Figure 1 is adequate and precise enough to represent the transformer power transferring and instantaneous load change phenomena and so, it's adequate for power electronics application without any further complexity addition [28].

The windings resistance R_d has a small value and can be determined with a DC source (ohmmeter). Nevertheless, in high frequency, the skin and proximity effect must be taken in consideration [29] [30]. The transformer of this work uses litz wire to minimize the skin effect [31]. The AC resistance would be almost 64% more than the DC value for the solid conductor at 20 kHz, while it is only 19.1% with the use of litz wire, about 3 times less.

The R_p value can be estimated using an adaptation of the Steinmetz's equation [32] and has a high value. The data from the manufacturer allows estimating the losses and so, the equivalent shunt resistance.

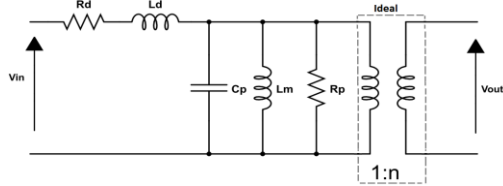


Fig. 1. Lumped model representation of the HV transformer.

Neglecting the core saturation, the remaining parameters are estimated through spectral analysis, applying a sinusoidal signal at the primary, with the secondary in open load condition. With the measurement of the primary voltage and current, the input impedance can be determined.

In low frequency range, the winding capacitance can be neglected, because of its high reactance. The resulting input impedance is the sum of the magnetizing and leakage reactances. As the magnetizing inductance is much higher than the leakage's, its approximated value is determined.

Using the same approach in the high frequency, where the capacitive reactance is so small that cancels the effect of the magnetizing inductance, the equivalent input impedance is only due to the leakage reactance. After this calculation, the magnetizing inductance is determined more precisely.

The low frequency resonance f_p (parallel resonance) occurs between L_m and C_p . At this point the maximum input impedance regards R_p . Nevertheless, as this essay uses a low voltage source, it's difficult to get the correct value of R_p .

Above this frequency, the input impedance presents a capacitive behavior. The high frequency resonance f_s (series resonance) occurs between L_d and C_p and gives the minimum input impedance. This minimum value represents the resistance at this frequency, which, due to the skin effect, doesn't represent the resistance at lower frequencies.

The C_p value can be calculated using both parallel and series resonances by (1) and (2) respectively, and the values must be close. The transformer's input impedance and the voltage gain are given by (3) and (4) respectively.

$$C_p = \frac{1}{(2\pi f_p)^2 L_m} \quad (1)$$

$$C_p = \frac{1}{(2\pi f_s)^2 L_d} \quad (2)$$

$$Z_{in} = \frac{R_d + s \left[L_d + L_m \left(1 + \frac{R_d}{R_p} \right) \right] + s^2 L_m \left(\frac{L_d}{R_p} + C_p R_d \right) + s^3 L_d L_m C_p}{1 + s \frac{L_m}{R_p} + s^2 L_m C_p} \quad (3)$$

$$\frac{V_{in}}{V_{out}} = \frac{snL_m R_p}{R_p R_d + s [R_d L_m + R_p (L_d + L_m)] + s^2 L_m (L_d + R_d R_p C_p) + s^3 R_p L_m L_d C_p} \quad (4)$$

A. Transformer's Parameters

The analysis uses the 1 kVA, 311 V, 20 kHz ferrite transformer showed in Figure 2. The core has a cross-section of 6.4 cm² and maximum flux density of 0.15 T. The primary and secondary number of turns are respectively 42 and 512, so the voltage ratio is 12. The secondary is divided in two equal layers, with the primary between them, improving the magnetic coupling. A signal generator feeds the primary, the secondary is open. Figure 3 shows the primary waveforms at 1 kHz.

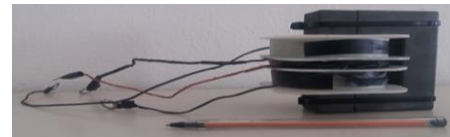


Fig. 2. HF HV transformer used in the spectral analysis performed in this section and in the experimental measurements.

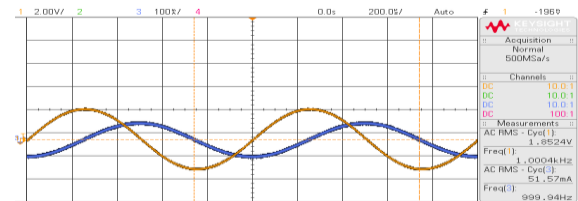


Fig. 3. Primary voltage (yellow) and current (blue) at low frequency range, used to estimate the magnetizing inductance value.

Figure 4 shows the situation at 50 kHz, the parallel resonance, in which the primary current achieves its minimum value. At 411 kHz occurs the series resonance. Figure 5 shows this situation, regarding the minimum input impedance. After the series resonance the input impedance presents an inductive behavior, as shown in Figure 6. The leakage inductance can be estimated at frequencies higher than the series resonance. Table I summarizes the estimated parameters for the model of Figure 1.

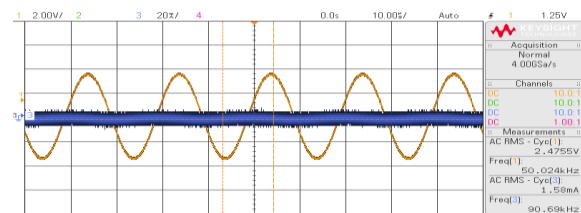


Fig. 4. Primary voltage (yellow) and current (blue) at the parallel resonance.

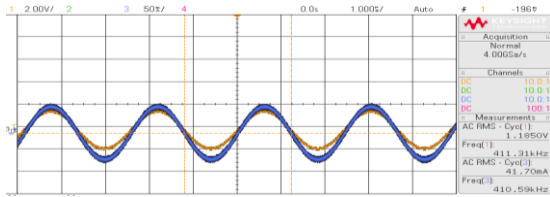


Fig. 5. Primary voltage (yellow) and current (blue) at the series resonance.

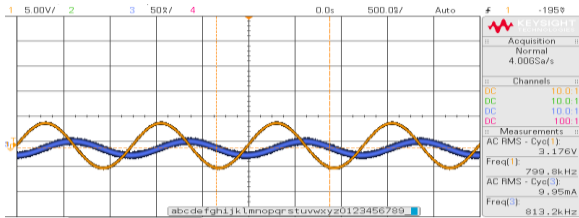


Fig. 6. Primary voltage (yellow) and current (blue) used to determine the leakage inductance.

TABLE I

Estimated Parameters for the Model of Figure 1

Parameter	Value
R_d	0.329 Ω
L_d	63.5 μ H
C_p	2.3 nF
L_m	5.64 mH
R_p	880 Ω
f	20 kHz
f_s	411 kHz
f_p	50 kHz
n	12

The windings capacitance calculated by (1) and (2) are 1.8 nF and 2.3 nF, respectively. One of the reasons for the discrepancy is the secondary leakage inductance, that's not considered in the model [28] [33]. The considered value is 2.3 nF, since the critical situation is the excitation of the series resonance, that produces secondary overvoltage and primary overcurrent.

Figures 7 and 8 show the behavior of the input impedance and the voltage gain respectively for the open and nominal load, obtained from (3) and (4) with the parameters of Table I. The input impedance of Figure 7 could be directly obtained from an impedance analyzer, and so the transformer inductances and capacitances directly estimated from it [34], however the spectral analysis as it was performed reproduces the analyzer behavior with the use of simple devices, as signal generator and oscilloscope.

Figure 9 shows the waveforms for open load condition. The harmonics in the square input voltage nearest the series resonance are amplified and distort the secondary voltage, that achieves a peak more than two times the expected value. The magnetizing current is also affected by the resonance manifestation, causing the current stress shown in Figure 9.

The load has an important role for minimizing such behavior. As it appears in parallel with the magnetizing branch, it damps the series resonance. However, if the transformer operates without load, some procedure must be adopted in order to comply with the isolation capability.

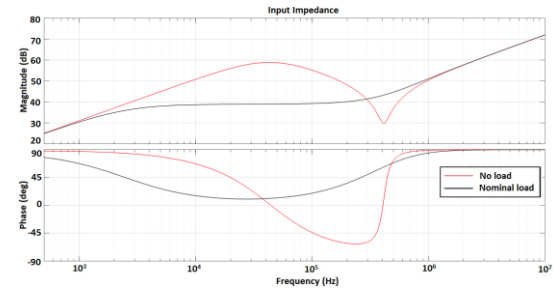


Fig. 7. Transformer's input impedance.

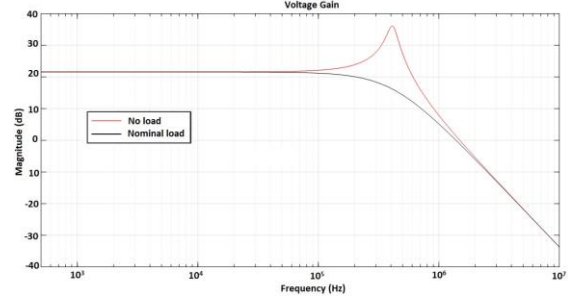


Fig. 8. Transformer's voltage gain.

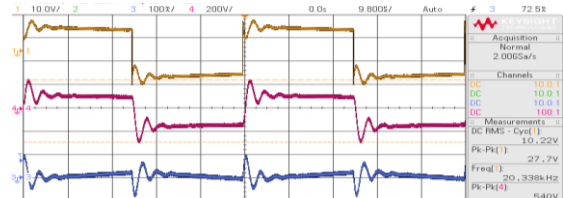


Fig. 9. Primary Voltage (yellow), Secondary Voltage (pink) and Primary current (blue), for the secondary open load condition.

III. RESONANCE EXCITATION AND PROTECTION STRATEGIES

Figure 10 shows a full bridge inverter feeding a HF HV transformer with a variable resistive load. The series capacitor C_{ext} blocks DC components from the inverter, avoiding the transformer saturation [35]. The transformer parameters are the same of Table I, R_L is a resistive variable load. The inverter parameters are listed in Table II.

Figure 11 shows the secondary voltage and the primary current for a PSIM simulation of Figure 10, with the parameters estimated by the spectral analysis. When the secondary is in open load condition, the primary current is the magnetizing current plus the resonant component, not damped by the load. The voltage peaks are more than two times the nominal voltage. This situation leads to the necessity of an overvoltage protection strategy, since the cost for increasing the isolation capability would be excessive.

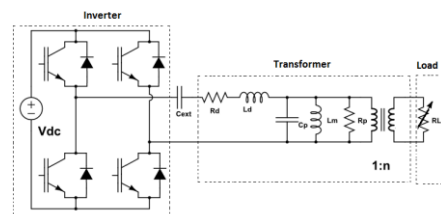


Fig. 10. Inverter feeding the transformer with a variable resistive load.

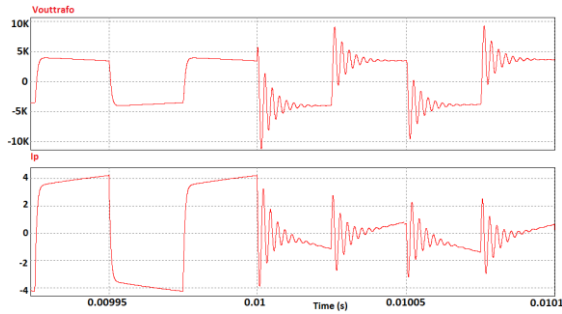


Fig. 11. Simulated waveforms of the transformer secondary voltage (top) and input current (bottom) for nominal power and open load conditions.

TABLE II

Inverter's Parameters of Figure 10	
Parameter	Value
V_{dc}	311 V
C_{ext}	2 μ F
Switching frequency	20 kHz

A. Voltage Clamper

Since the capacitance, C_p is unreachable, it's impossible to, directly, limit its voltage. As such voltage is applied to the magnetizing inductance, it appears on the secondary side. To limit the voltage during open load operation, a voltage clamper [36] can be put at the secondary, as Figure 12 shows.

The clamper uses high voltage high frequency diodes, a high voltage capacitor (C_{cl}) and enough resistive load (R_{cl}). During normal operation, the capacitor charges with the nominal voltage. During the resonance, the clamper absorbs the energy associated with the L_d - C_p tank and dissipates it on the resistor. There's a slightly increase peak voltage, but the AC output remains limited. Figure 13 shows the primary current and secondary voltage, for nominal and open load conditions with the clamper. The clamper resistance must be high to limit the losses but not so high in order to limit the overvoltage. Main drawbacks of this solution are the cost of HF HV components as well as the additional losses.

B. External Inductor

If the leakage inductance would be zero, the inverter would impose directly the voltage on the magnetizing branch, and no overvoltage would occur, even in the open load condition. However such ideal case is impossible, it can be approximate if the leakage inductance has a small value. In such situation an external inductor can be connected in series with the primary. Its value must be significantly higher (as around two to ten times) than the leakage inductance. The value can't be excessively high to not limit the primary current and, consequently, the power transfer.

The point between the inductor and the transformer is connected to the intermediary point of a diodes branch and connected to the inverter's DC link as Figure 14 shows [37].

The diodes branch operates as a clamper and limits the voltage on the primary to $\pm V_{dc}$. As the leakage inductance is small compared to the external inductor, the voltage at the magnetizing branch and at the output is limited, reducing the transformer high voltage peaks.

Figure 15 shows the output voltage limitation with the external inductor. The main drawback of this solution is the power factor reduction, due to higher series inductance. So, for a given output power, the input current will be higher than without the external inductor.

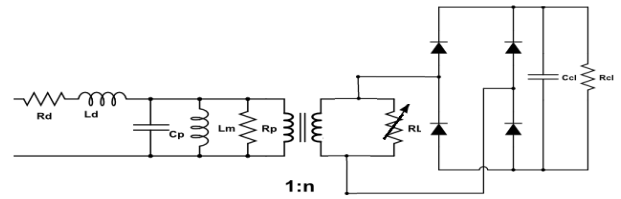


Fig. 12. System of Figure 11 with the voltage clamper at the secondary side.

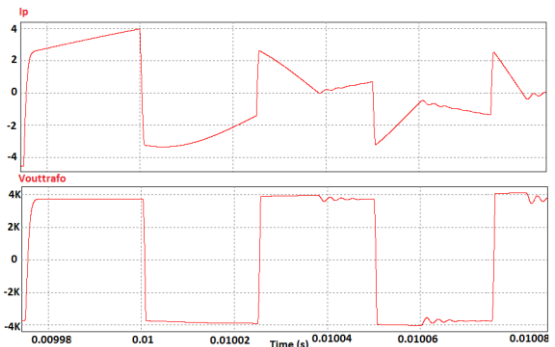


Fig. 13. Input current (top) and secondary voltage (bottom) with the clamper at open load.

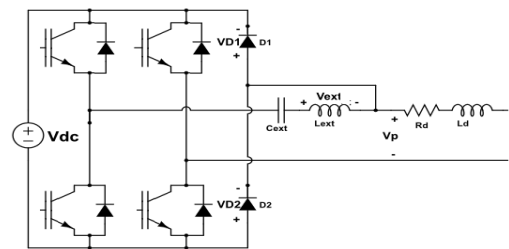


Fig. 14. External inductor strategy.

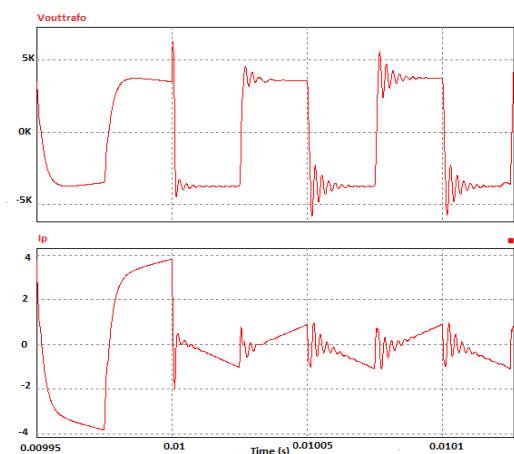


Fig. 15. Secondary voltage (top) and primary current (bottom) with the external inductor.

C. Harmonic Reduction

The series resonance won't be excited if the primary voltage doesn't have the respective harmonic. Without compromising the switching frequency, it's possible to

produce a three-level waveform, including a zero-voltage step. The length of the zero interval allows eliminating one specific harmonic. For example, if the zero-voltage interval is 1/21 of the period, the 21st harmonic is cancelled.

Figure 16 shows the primary and secondary voltages and the primary current for this strategy, the 21th harmonic was removed from the input signal, because the series resonance frequency is 411 kHz and the operating frequency is 20 kHz.

As expected, the overvoltage has been reduced. The oscillation is the 19th harmonic that remains in the applied rectangular voltage. The elimination of additional harmonics is possible, at the cost of increase the transistors switching frequency [38] [39] [40].

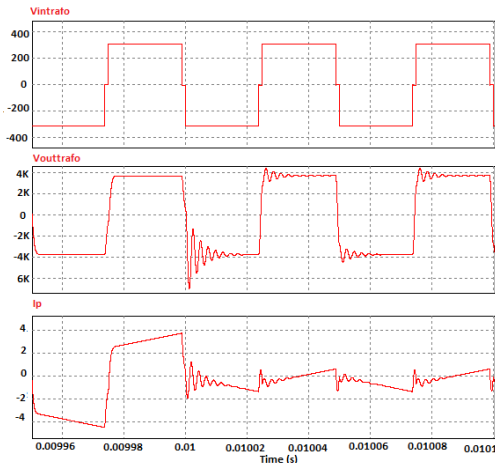


Fig. 16. From top to bottom: Primary voltage; secondary voltage and primary current for the harmonic control strategy.

IV. CRITERIA DESIGN FOR THE PROTECTION STRATEGIES

A. Voltage Clamper

The magnetizing current with the series resonance manifestation is shown in Figure 17. The magnetizing current peak with the resonance manifestation is I_p . This value is achieved in a quarter of the wave-cycle at the resonant frequency. To determine I_p , the “natural” magnetizing current peak I_m must be taken in consideration and its value subtracted from the total current in the resonant circuit. The value of I_m can be estimated using the switching frequency, the DC link and L_m values.

The resonant circuit may be regarded as a simple LC without losses. Its characteristic impedance is given by (5), the total current is given by (6) and I_p is calculated by (7).

$$Z_c = \sqrt{\frac{L_d}{C_p}} \quad (5)$$

$$I_c = \frac{2V_{dc}}{Z_c} \quad (6)$$

$$I_p = I_c - I_m. \quad (7)$$

The total charge delivered by the “resonant current” during this time interval is calculated by (8) and determined

by (9). Considering the transformer secondary can handle an overvoltage ΔV , the clamper capacitor is given by (10).

$$Q_s = 2 \int_0^{\frac{1}{2f_s}} I_p \sin(2\pi f_s t) dt \quad (8)$$

$$Q_s = \frac{2I_p}{\pi f_s} \quad (9)$$

$$C_{cl} = \frac{2I_p}{\pi f_s \Delta V}. \quad (10)$$

The energy absorbed by C_{cl} in a half period is given by (11) and must be dissipated on the clamper resistor. Considering the voltage on the resistor constant and equals to V_o , the power dissipate during the resonance is given by (12), and its value can be calculated by (13).

$$E_s = \frac{I_p \Delta V}{\pi f_s} \quad (11)$$

$$P_{R_{cl}} = \frac{E_s}{T/2} \quad (12)$$

$$R_{cl} = \frac{(V_o)^2 \pi f_s}{2I_p \Delta V f} \quad (13)$$

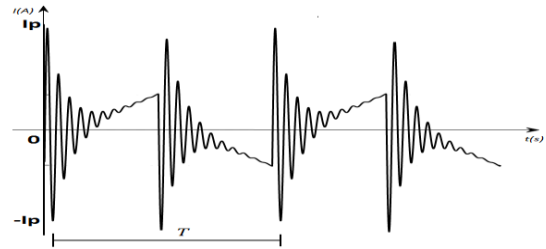


Fig. 17. Magnetizing current with the series resonance manifestation.

For the 1 kVA ferrite transformer, the output voltage at normal operation is 3.8 kV. The magnetizing current is 0.69 A, the characteristic impedance 164 Ω and the total resonant peak current 3.79 A. The I_p value is 3.10 A. The clamper parameters, considering an overvoltage of 200 V are showed in Table III.

TABLE III

Determined Parameters for the High Voltage Clamper	
Parameter	Value
C_{cl}	24 nF
R_{cl}	748.29 k Ω

B. External Inductor

Figure 18 shows the waveforms for the external inductor and the primary voltage at nominal conditions, as well as the inverter output voltage.

During the positive half-cycle, the inverter’s output is V_{dc} . The external inductor is initially uncharged, behaving as an open circuit with a voltage drop higher than V_{dc} . The primary voltage is the difference between the inverter and inductor

voltages, so it is 0. The voltage on D_1 and D_2 are $-V_{dc}$ and 0 respectively, as seen in Figure 18. The higher initial voltage on the external inductor is due to C_{ext} effect.

As the inductor charges, its voltage tends to zero and the primary increases gradually to V_{dc} . The voltages on D_1 and D_2 tend to 0 and $-V_{dc}$ respectively. When the semi-cycle changes, the behavior is similar, but the voltage values are opposite, as seen in Figures 18 and 19. The primary, inductor and diode currents are also shown in Figures 20 and 21, for the open load condition. There's a slight difference between the inductor and primary currents, because of the current circulation trough the diodes. The diodes polarization depends on the voltage at the point between the external inductor and the primary.

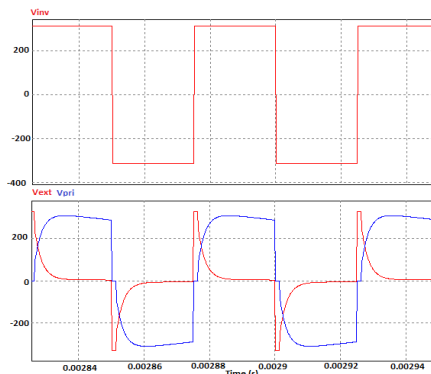


Fig. 18. From top to bottom: Inverter output voltage; Primary and external inductor voltages, at nominal conditions.

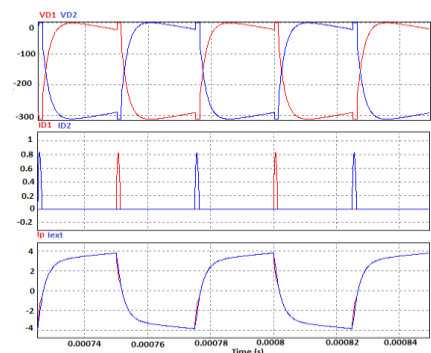


Fig. 19. From top to bottom: Diodes voltages; Diodes current; Primary and external inductor currents, for the external inductor strategy at nominal conditions.

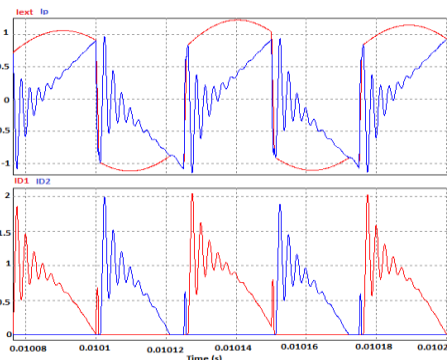


Fig. 20. Waveforms for the external inductor strategy at open load condition. From top to bottom: Primary and inductor currents; Diode currents.

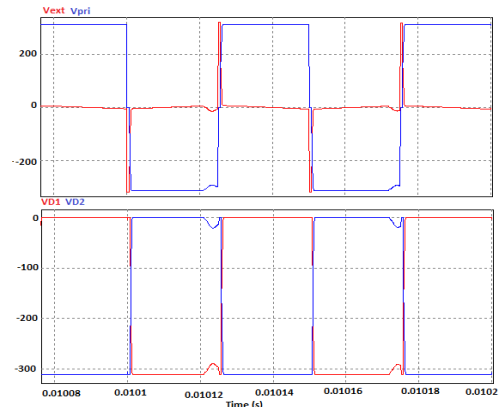


Fig. 21. Voltages at open load condition. From top to bottom: Primary and external inductor; Diodes.

If the leakage inductance is high, this solution can't be applied. Table IV shows the output power obtained from simulations of the external inductor strategy with nominal load at the secondary and the respective voltage peak in the open load condition. It can be seen that higher the external inductor, lower the open load voltage peak, but lower the power delivered and the output RMS voltage. The results confirm that the best system performance (more overvoltage and less output power reduction) is when the inductor is nearly between around two to ten times the leakage inductance.

TABLE IV

Power and Voltage Variation With the External Inductor			
External Inductor	Outut Voltage rms value	Output Power	Secondary open voltage peak
0 μ H	3.68 kV	944 W	9.2 kV
100 μ H	3.46 kV	834 W	6.3 kV
150 μ H	3.34 kV	778 W	5.8 kV
200 μ H	3.21 kV	720 W	5.2 kV
300 μ H	2.96 kV	610 W	4.5 kV
600 μ H	2.22 kV	350 W	3.8 kV

C. Harmonic Reduction

The waveform is shown in Figure 22, the half-wave and odd symmetry result the Fourier series given by (14). The Fourier coefficients are given by (15), with t_l being the zero interval per half-period and determined by (16). By putting (16) in (15), the expression in (17) is derived. Not only b_N , but all the harmonics multiple of N are eliminated.

A drawback of this solution is the reduction of the applied RMS voltage, which impacts the power transfer. For the 1 kVA transformer, the output power is 899 W. When this strategy is used, it's necessary to redesign the transformer for the specific input voltage waveform.

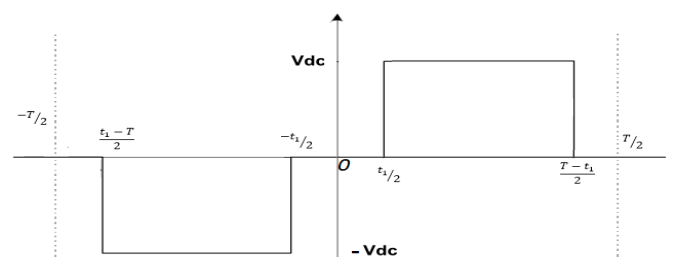


Fig. 22. Square wave with zero-step.

$$f(t) = \sum_{n=1}^{\infty} b_n \sin \frac{2\pi n t}{T} \quad (14)$$

$$b_n = \frac{4V_{dc}}{\pi n} \cos \frac{\pi n t_1}{T} \quad (15)$$

$$t_1 = \frac{T}{2N} \quad (16)$$

$$b_n = \frac{4V_{dc}}{\pi n} \cos \frac{\pi n}{2N} \quad (17)$$

V. EXPERIMENTAL RESULTS

Figure 23 shows the prototype, where it's seen the HF HV transformer, the voltage inverter, the HV clamber and the measurement setup. A high voltage probe Tektronix P 6015A is used to measure the secondary voltage. The probe has a capacitance of 3 pF, that changes the resonance frequency to nearly 380 kHz, reducing the tank circuit impedance and increasing the resonant current. So, there will be some mismatches between simulations and experimental results.



Fig. 23. Experimental setup for the practical measurements of the overvoltage protection strategies.

Figure 24 shows the primary waveforms for a resistive load of 12.5 kΩ and Figure 25 the respective secondary voltage. The input power was almost 1.1 kW.

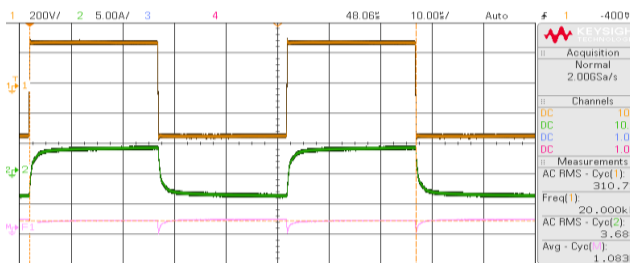


Fig. 24. Primary voltage (yellow), primary current (green) and input power (pink) for a resistive load of 12.5 kΩ.

Figure 26 shows the primary waveforms for a load of 75 kΩ and Figure 27 the corresponding secondary voltage. The secondary approximates the open load condition when the load value increases, reducing the damping and increasing

primary current and secondary voltage peaks. In this case, the voltage peak is already two times the value of Figure 25.

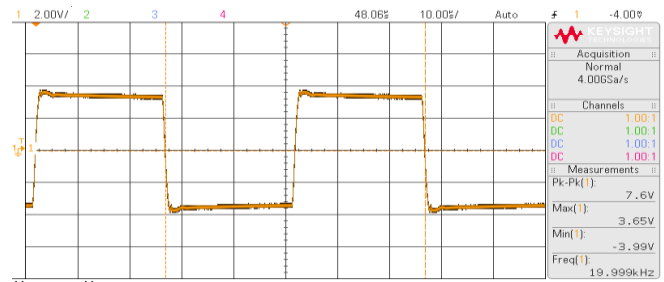


Fig. 25. Secondary voltage corresponding to the primary waveforms of Figure 24. Vertical scale 1:1000.

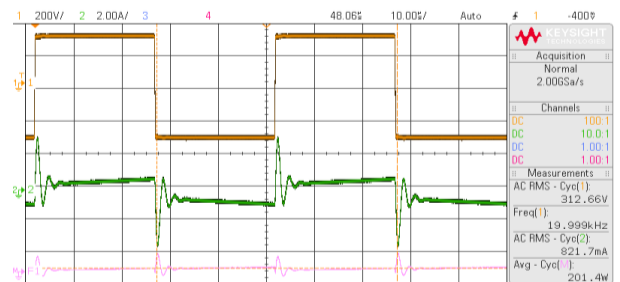


Fig. 26. Primary voltage (yellow), primary current (green) and input power (pink) for a resistive load of 75 kΩ.

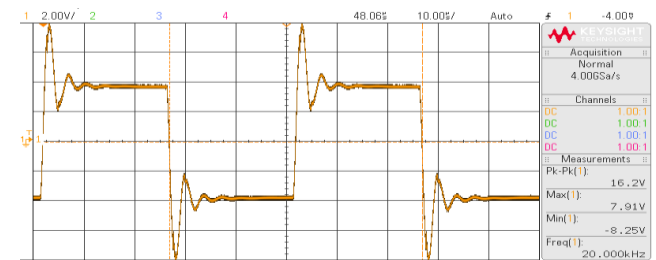


Fig. 27. Secondary voltage for the primary waveforms of Figure 26. Vertical scale 1:1000.

A. Secondary Clamber

The primary waveforms for the HV clamber strategy at the open load condition are showed in Figure 28 and the corresponding secondary voltage in Figure 29, For the clamber capacitor prototyping it was used a combination of five capacitors of 4.7 nF in parallel and, for the resistor, eight of 100 kΩ in series. The secondary voltage peak is nearly 4.5 kV and the primary current peak almost 5 A. The waveforms show the effectiveness of this strategy. The input power was 56.2 W, 5.62% of the nominal power.

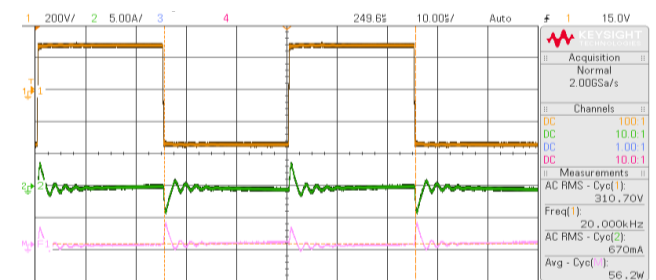


Fig. 28. Primary waveforms for the voltage clamber strategy. From top to bottom: Primary voltage, Primary current and input power.

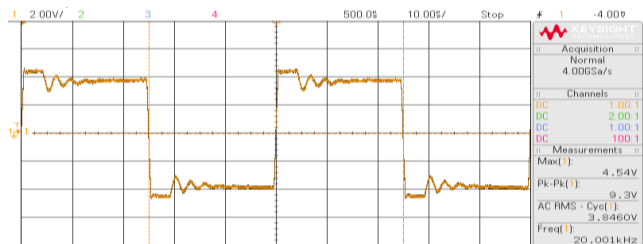


Fig. 29. Secondary voltage for the clamber strategy. Vertical scale 1:1000.

B. External Inductor

Figure 30 shows the primary waveforms for the external inductor strategy at the open load condition, and Figure 31 the corresponding secondary voltage, the external inductor value is 150 μ H. The secondary voltage peak was 4.5 kV and the primary current peak less than 2 A. The input power was 10.2 W.

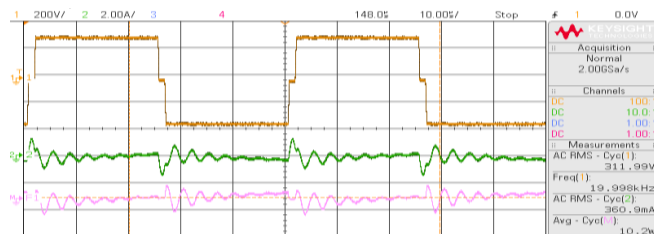


Fig. 30. Primary voltage (yellow), Primary current (green) and input power (pink) for the external inductor strategy, with the secondary in the open load.

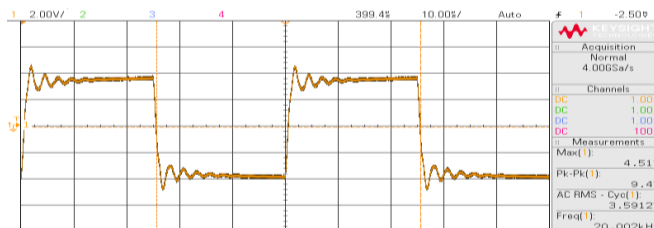


Fig. 31. Secondary Voltage in the open load condition for the external inductor strategy. Vertical scale 1:1000.

C. Harmonic Control

Figure 32 shows the primary waveforms for the selective harmonic elimination and Figure 33 the corresponding secondary voltage for the open load condition. As the primary voltage period is 50 μ s and the harmonic to be eliminated is the 21st, the value of t_i determined by (16) is 1.19 μ s. The secondary voltage peak was about 4.3 kV and the primary current peak almost the same as in the external inductor strategy. The input power was less than 20 W. The waveforms show the effectiveness of this strategy.

Table V summaries some important information about the protection strategy. The external inductor and voltage clamber have similar performance in terms of overvoltage reduction. The external inductor has less power loss, but can only be applied if the leakage inductance has a small value, as the voltage clamber does not have this project restriction.

The harmonic elimination had the best overvoltage reduction, but it can't be applied if the series resonance happens in harmonics too far from the switching frequency.

The harmonic elimination and external inductor reduce the

power transfer, once they decrease the RMS value of the primary voltage, so besides the overvoltage protection, the application efficiency necessity must be taken in consideration.

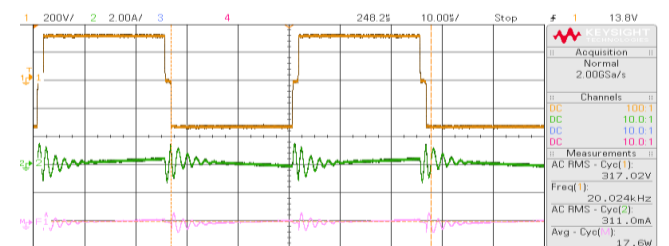


Fig. 32. Primary waveforms for the selective harmonic elimination.

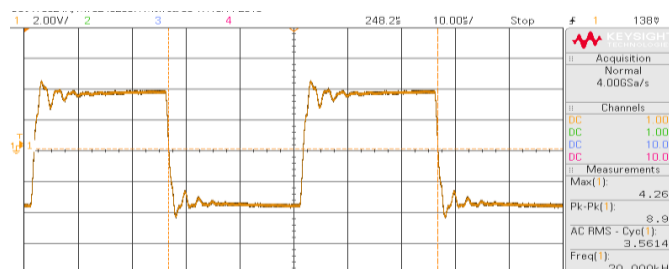


Fig. 33. Secondary voltage corresponding to the selective harmonic elimination strategy. Vertical scale 1:1000.

TABLE V

Comparison Among the Overvoltage Protection Strategies for Open Load

Strategy	Secondary Overvoltage (% above expected rated voltage)	Input Power Loss (% of rated power)	Primary Current Peak (A)	Primary Current RMS Value (A)
Voltage Clamber	18.4%	5.62%	4	0.67
External Inductor	18.4%	1%	1.8	0.36
Harmonic Reduction	13.1%	2%	1.8	0.31

VI. CONCLUSIONS

In this paper the nature and problems of overvoltage in the open circuit operation of High Voltage High Frequency transformers were explored and different protection strategies to limit the voltage stress were proposed, depending on the transformer parasitic elements values, mainly the leakage inductance and the windings capacitance. The strategies apply in situations in which the load varies instantaneously, asking for an overvoltage protection implemented in hardware, since no closed loop control would be so fast in order to protect the devices.

The strategies were simulated and validated by experimental results. The operation of each strategy was analyzed, and design criteria were established.

The high voltage probe capacitance impacts the measurements, however it doesn't affect the comparison, since all the results were acquired at the same conditions. The probe capacitance probably is one of the reasons for the damping differences between the measured and simulated

waveforms. Another reason could be system losses that were not modeled. For sure, the lumped parameters model is not able to perfectly represent the internal behavior of the transformer, although it represents with a good precision the power transferring phenomena.

The external inductor is the simplest strategy, but it's only indicated when the leakage inductance value is small. The selective harmonic elimination is more effective if the series resonance happens in a low frequency range. The HV clamper has the disadvantage of HF HV components necessity and can be expensive in high power applications.

ACKNOWLEDGEMENTS

The authors acknowledge Zasso Brazil for financially supporting this research.

REFERENCES

- [1] L. A. F. d. Oliveira, *Study of High Frequency Transformer Models* (in Portuguese), Belo Horizonte, MG: UFMG, June 2011.
- [2] C. W. T. McLyman, *Transformer and Inductor Design Handbook*, 3 ed., New York: Marcel Dekker Inc, 2004.
- [3] R. Petrov, "Optimum Design of High-Power, High-Frequency Transformer", in *IEEE Transactions on Power Electronics*, vol. 11, no. 1, p. 33-42, January 1996.
- [4] A. R. A. Razak and S. Tajb, "Design considerations of a high frequency power transformer," in *National Power Engineering Conference (PECon)*, Bangi, December 2003.
- [5] J. A. Pomilio, O. Bet and M. P. Vieira, "High-Voltage Resonant Converter with Extreme Load Variation: Design, Criteria and Applications", in *International Journal of Electrical, Computer, Electronics and Communication Engineering*, vol. 8, no. 12, p. 1764-1769, 2014.
- [6] H. Y. Lu, J. G. Zhu, V. S. Ramsden and S. Y. R. Hui, "Measurement and Modeling of Stray Capacitances in High Frequency Transformers", in *IEEE Power Electronics Specialists Conference*, p. 763-768, 1 July 1999.
- [7] H. Y. Lu, J. G. Zhu and S. Y. R. Hui, "Experimental Determination of Stray Capacitances in High Frequency Transformers", in *IEEE Trans. on Power Electronics*, vol. 18, no. 5, p. 1105-1112, September 2003.
- [8] G. S. Sperandio and J. A. Pomilio, "High-efficiency, high-frequency inverter for silent discharge load", in *Brazilian Power Electronics Conference*, Blumenau, October 2007.
- [9] D. Tardivo and J. A. Pomilio, "Resonant High-voltage supply for multiple paralleled loads with parameter equalization", in *Brazilian Power Electronics Conference*, Natal, September 2011.
- [10] W. Shen, *Design of High-Density Transformers for High-Frequency High-Power Converters*, Blacksburg, Virginia: Virginia Polytechnic Institute State University, July 2006.
- [11] W. Shen, F. Wang, D. Boroyevich and C. W. Tipton, "High power density nanocrystalline core transformer design for resonant converter systems", in *40th Industry Applications Conf.*, vol. 3, p. 2216-2222, October 2005.
- [12] M. A. Perez, C. Blanco, M. Rico and F. Linera, "A New Topology for High Voltage High Frequency Transformers", in *IEEE Applied Power Electronics Conference and Exposition*, vol. 2, p. 554-559, March 1995.
- [13] M. Biberoglu, T. N. Gücin and B. Fincan, "Analyzing the influences of high frequency transformers utilized in parallel resonant converters", in *IEEE International Conference on Renewable Energy Research and Applications*, p. 983-988, November 2016.
- [14] A. Atalla, M. Agamy, M. Dame, L. Hao, G. Mandrasiak and Y. Pan, "Advancements in high power high frequency transformer design for resonant converter circuits", in *IEEE Energy Conversion Congress and Exposition*, p. 1-8, September 2016.
- [15] O. Patterson and D. Divan, "Pseudo-Resonant Converter Technologies", in *IEEE 18th Power Electronics Specialists Conference*, Blacksburg, June 1987.
- [16] A. Mizuno, A. Nagura, T. Miyamoto, A. Chakrabarti, T. Sato, K. Kimura, T. Kimura and M. Kobayashi, "A portable weed control device using high frequency AC voltage", in *IEEE Industry Applications Conference*, vol. 3, p. 2000-2003, October 1993.
- [17] S. Mao, J. Popovic and J. A. Ferreira, "An Investigation into High Frequency High Voltage Planar Transformer for High Voltage Generator Applications", in *IEEE International Conference on Integrated Power Electronics Systems*, p. 1-6, March 2016.
- [18] Y. A. Wang and D. M. Xiao, "Prototype design for a high-voltage high-frequency rectifier transformer power use", in *IET Power Electronics*, vol. 4, no. 6, p. 615-623, July 2011.
- [19] J. Baizan, A. Navarro-Crespin, R. Casanueva, F. J. Azcondo, C. Brañas and F. J. Diaz, "Converter with four quadrant switches for EDM Applications", in *IEEE Industry Applications Annual Meeting*, October 2013.
- [20] R. Casanueva, C. Brañas, F. J. Azcondo and S. Bracho, "Resonant converters: properties and applications for variable loads", in *31st Annual Conference of IEEE Industrial Electronics Society*, November 2005.
- [21] S. de Andrade Coutinho Filho, J. A. Pomilio, B. Valverde and D. Teruo Mendes de Souza, "Weed Inactivation Device". Patent WO/2019/102243, 2019.
- [22] D. T. M. Souza, B. Valverde and J. A. Pomilio, "Overvoltage protection procedures for high frequency high voltage transformers", in *14th Brazilian Power Electronics Conference (COBEP)*, Juiz de Fora, November 2017.
- [23] F. D. Leon and A. Semlyen, "Efficient calculation of elementary parameters of transformers", in *IEEE Transactions on Power Delivery*, vol. 7, no. 1, p. 376-383, January 1992.
- [24] M. M. Kane and S. V. Kulkarni, "MTL-Based analysis to distinguish high-frequency behavior of interleaved

- windings in power transformers", in *IEEE Trans. on Power Delivery*, vol. 28, no. 4, p. 2291-2299, July 2013.
- [25] H. Y. Lu, J. G. Zhu and S. Y. R.Hui, "Experimental determination of stray capacitances in high-frequency transformers", in *IEEE Transactions on Power Electronics*, vol. 18, no. 5, p. 1105-1112, August 2003.
- [26] J. Bielar and J. W. Kolar, "Using transformer parasitics for resonant converters-a review of the stray capacitance of transformers", in *IEEE 40th Industry Applications Conference*, vol. 3, p. 1868-1875, October 2005.
- [27] B. Cogitore, J. P. Keradec and J. Barbaroux, "The two-winding transformer: experimental method to obtain a wide frequency equivalent circuit", in *IEEE Transactions on Instrumentation and Measurement*, vol. 43, no. 2, p. 364-371, April 1994.
- [28] D. T. M. Souza and J. A. Pomilio, "Comparison between lumped models for high-voltage high-frequency transformers", in *13th IEEE International Conference on Industry Applications (INDUSCON)*, São Paulo, November 2018.
- [29] P. Mayer, P. Germano and Y. Perriard, "FEM modeling of skin and proximity effects for coreless transformers", in *IEEE 15th International Conference on Electrical Machines and Systems (ICEMS)*, p. 1-6, October 2012.
- [30] A. Roßkopf, E. Bär and C. Joffe, "Influence of Inner Skin and proximity Effects on Conduction Litz Wires", in *IEEE Transactions on Power Electronics*, vol. 29, no. 10, p. 5454-5461, October 2014.
- [31] C. R. Sullivan and R. Y. Zhang, "Simplified Design Method for Litz Wire", in *IEEE Applied Power Electronics Conference and Exposition*, p. 2667-2674, April 2014.
- [32] S. A. D. Contreras, *Study of the Application of Intercellular Transformers in Voltage Inverters* (in Portuguese), Belo Horizonte, MG: UFMG, July 2014.
- [33] N. Shafiei, M. Pahlevaninezhad, H. Farzanehfard, A. Bakhshai and P. Jain, "Analysis of a Fifth-Order Resonant Converter for High-Voltage DC Power Supplies", in *IEEE Transactions on Power Electronics*, Vol.28, N.1, p. 85-100, January 2013.
- [34] G. L. Piazza, R. L. Alves, C. H. I. Font and I. Barbi, "Resonant circuit model and design for a high frequency high voltage switched-mode power supply", in *10th Brazilian Power Electronics Conference (COBEP)*, Bonito, September 2009.
- [35] J. P. Bonaldo, *Power Converter Feeding Ozone Generation Cells* (in Portuguese), Campinas, SP: Unicamp, April 2010.
- [36] J. Rocabert, M. M. Dumenjo, J. Bordonau and J. A. B. Jimenez, "A regenerative active clamp circuit for DC/AC converters with high-frequency isolation in photovoltaic systems", in *IEEE 35th Annual Power Electronics Specialists Conference*, vol. 3, p. 2082-2088, June 2004.
- [37] F. Tsai and F. C. Lee, "A complete dc characterization of a constant-frequency, clamped-mode, series-resonant converter", in *IEEE 19th Power Electronics Specialists Conference*, Kyoto, April 1988.
- [38] S. Bhadra, D. Grogory and H. Pitangia, "An analytical solution of switching angles for Selective Harmonic Elimination (SHE) in a cascaded seven level inverter", in *IEEE 2nd Southern Power Electronics Conference*, Auckland, December 2016.
- [39] M. S. A. Dahidah, G. Konstantinou and V. G. Agelidis, "A Review of Multilevel Selective Harmonic Elimination PWM: Formulations, Solving Algorithms, Implementation and Applications", in *IEEE Transactions on Power Electronics*, vol. 30, no. 8, p. 4091-4106, August 2015.
- [40] N. V. Kumar, V. K. Chinnaiyan, M. Pradish and M. S. Divekar, "Selective harmonic elimination: An comparative analysis for seven level inverter", in *IEEE Students' Technology Symposium (TechSym)*, Kharagpur, October 2016.
- [41] C. K. Alexander and M. N. O. Sadiku, *Fundamentals of Electric Circuits*, 5th ed., New York: McGraw-Hill, 2013.
- [42] E. M. Stein and R. Shakarchi, *Princeton Lectures in Analysis I Fourier Analysis An introduction*, New Jersey: Princeton University Press, 2002.

BIOGRAPHIES

Diego Teruo Mendes de Souza was born in Ferraz de Vasconcelos, SP, Brazil, on January 9th, 1992. He received the B.S. in Electrical Engineering from the Federal University of Viçosa (UFV), Viçosa, MG, Brazil in 2016 and the M.S. from University of Campinas, Brazil, in 2018. He is currently professor at the Faculty of Americana and R&D Engineer at Zasso Brazil. His research fields of interest include: Power Electronics, Electromagnetism, Control Engineering, Power Grid.

Bruno Valverde was born in Jundiaí, Brazil, in 1990. He received the B.S. degree in Electrical Engineering from the Federal University of São Carlos (UFSCar), São Carlos, Brazil, in 2016 and the M.S. from University of Campinas, Brazil, in 2019. He is currently R&D Engineer at Zasso Brazil. His research fields of interest include Power electronics, More Electric Aircraft systems, high voltage resonant sources and Microgrids.

José Antenor Pomilio (M'92–SM'02) was born in Jundiaí, Brazil, in 1960. He received the B.S., M.S., and Ph.D. degrees in electrical engineering from the University of Campinas, Brazil, in 1983, 1986, and 1991, respectively. From 1988 to 1991, he was the Head of the Power Electronics Group, Brazilian Synchrotron Light Laboratory. He was a Visiting Professor with the University of Padova, in 1993 and 2015 and with the Third University of Rome, in 2003, both in Italy. He is a Professor with the School of Electrical and Computer Engineering, University of Campinas, where he has been teaching since 1984. Dr. Pomilio was the President of the Brazilian Power Electronics Society in 2000–2002, member of the Administrative Committee of the IEEE Power Electronics Society in 1997–2002, and Associated Editor of the IEEE Transaction on Power Electronics in 2003-2018.